INVESTIGATION OF CHAR-SLAG INTERACTION REGIMES IN ENTRAINED-FLOW GASIFIERS: FROM EXPERIMENTAL EVIDENCE TO NUMERICAL SIMULATIONS

Fiorenzo Ambrosino*, Andrea Aprovitola, Paola Brachi***, Francesco Saverio Marra**, Fabio Montagnaro*** and Piero Salatino******

fabio.montagnaro@unina.it

* ENEA, CR Portici, Piazzale Enrico Fermi 1, 80055 Portici (Italy)

** Istituto di Ricerche sulla Combustione, CNR, Via Diocleziano 328, 80124 Napoli (Italy)

*** Dipartimento di Chimica, Università degli Studi di Napoli Federico II, Complesso Universitario di Monte Sant'Angelo, 80126 Napoli (Italy)

**** Dipartimento di Ingegneria Chimica, Università degli Studi di Napoli Federico II, Piazzale Vincenzo Tecchio 80, 80125 Napoli (Italy)

Abstract

Entrained-flow gasifiers are characterized by operating conditions that promote ash migration/deposition onto the reactor walls, whence the ash is drained as a molten phase. Previous investigations have shed light on the fate of char particles as they impinge on the wall slag layer: both char entrapment inside the melt and carbon-coverage of the slag can occur, as suggested by experimental investigation of ashes generated by full-scale plants. Because of the wide range of spatial and temporal scales involved in these phenomena, numerical simulation of the fate of the flying fine char particles is a very difficult task. Simulation is most frequently based on the RANS (Reynolds Averaged Navier Stokes Simulation) approach [1], in which the particle-boundary interaction needs to be modelled by means of empirical models that already postulate the leading interaction mechanism. On the other hand, application of more detailed models to full-scale configurations is computationally prohibitive. Therefore, detailed simulations based on a Eulerian LES (Large Eddy Simulation) approach [2] for the turbulent gas phase and a Lagrangian particle tracking approach for the solid phase have been performed to explore, in a simplified flow configuration, near-wall particle segregation and the role of relevant parameters. In this work, the role of the properties of the slag layer, specifically its inelastic behaviour, has been investigated. Results of numerical simulations have been critically discussed with reference to the experimental observations.

Introduction

Entrained-flow coal gasifiers of new generation are often characterized by operating conditions aimed at favouring ash migration/deposition onto the reactor walls, whence the molten ash (slag) flows and is eventually drained at the bottom of the gasifier [3,4]. In a recently published study [5], Montagnaro and Salatino have shed light on the fate of char particles as they impinge on the wall slag layer: from a theoretical point of view, it has been shown that either char entrapment inside the melt or carbon-coverage of the slag may occur, depending on properties like char density, particle diameter and impact velocity, slag viscosity, interfacial particle-slag tension. Occurrence of char entrapment prevents further progress of combustion/gasification. On the contrary, if char particles reaching the wall adhere to the slag layer's surface without being fully engulfed the progress of combustion/gasification is still permitted. In particular, if the coverage of the slag layer with carbon particles is extensive, a dense-dispersed annular phase may establish in close

proximity of the wall ash layer, where the excess impinging char particles which cannot be accommodated on the slag surface accumulate. This phase is likely to be characterized by a velocity that is intermediate between that of the fast lean-dispersed particle phase and that of the slowly moving wall molten ash layer. This feature is beneficial to C conversion as it gives rise to a longer mean residence time of carbon particles belonging to this phase.

The complex phenomenology associated with interaction of a particle-laden turbulent flow with the inelastic slag-covered wall of the gasifier has been the subject of numerical simulation. A major issue is represented by the appropriate level of detail which is required to represent the relevant phenomena: multiphase turbulent flow transport, particle-slag interaction, particle-particle interaction. Several full-scale and comprehensive numerical models of gasifiers have been recently presented [6]. These models incorporate the main features associated with the existence and dynamics of the particle phase into the CFD framework: mass transfer from the solid to the gas phases due to gasification, momentum and energy exchange between the particle and the gas phases, the course of heterogeneous and homogeneous chemical reactions. However, as the scales involved in the gasification processes range from sub-micron scale up to the integral scale of a gasifier reactor chamber (of the order of tens of meters), the use of subgrid scale models [2], mostly based on empirical correlations, becomes essential. With specific reference to the particle-wall interaction phenomena which are the main focus of the present study, several theories predicting the deposition rates of carbon and ash particles are available [7–10]. They provide useful information for design and engineering purposes, but they fall short when a detailed mechanistic frame for particle-wall interaction is needed.

The Eulerian-Lagrangian approach for the gas and particle phases, respectively, is a good compromise to predict particle dispersion in gas and to focus on the mechanisms of wall-particle interaction. To accurately predict the particle-slag interaction, a proper level of modelling has to be identified and adopted. In this work, it is proposed that a model based on the Large Eddy Simulation of the fluid phase, coupled with a proper Discrete Element Method for the solid phase, is an effective tool to investigate the interaction of a particle-laden gas flow and the slag-covered wall of the gasifier. This class of problems usually needs huge computational power due to both the high number of computational cells required to properly select the cut-off threshold of the LES filter, and the high number of particles to track. The LES is being preferred over the time-averaged RANS approach, as the resolved variable contains most of physical turbulent fluctuations which determine the coal and ash particle path, otherwise entirely modelled in the RANS approach. Furthermore, LES methods provide statistical information about the energy-containing flow scales, which is not available in RANS methods. It appears that LES method seems adequate to evaluate the response of the char particles to the momentum variation induced by the turbulence [11–13].

To limit the required computational effort, dimensions for reference quantities have to be carefully selected to obtain a Reynolds number and a number of particles limited to a few thousands. By properly sizing the extension of the computational domain, however, it is possible to satisfy these requirements and reproduce the key features of the dynamics of the particles interacting with the neighbouring phases. How this aspect is tackled is the subject of a separate paper [14]. Here some results obtained with this model are presented. Based on the numerical predictions and on experimental results concerning the properties of bottom ash from full-scale gasifier, the mechanism leading to near-wall char segregation and char/slag interaction may be inferred.

Properties of Bottom Ash from Full-Scale Gasifiers

In a parallel investigation [15], solid residues coming from an industrial-scale entrained-flow slagging gasifier have been characterized. The properties of the different ash streams have

been analyzed in the light of the different regimes of char-slag micromechanical interaction and of the different phases that are established in the gasification chamber. In this context, it is useful to remind that the solid waste other than fly ash is quenched in a water bath generating, besides the *slag* (sometimes referred to as *coarse slag*), a black water whence *slag fines* are recovered by filtration [16]. Only recently did the question concerning the differences between coarse and fine slag receive consideration: the reader is referred, for example, to the works of Wu et al. [16], Xu et al. [17] and Zhao et al. [18]. Samples of coarse slag and slag fines were generated in the ELCOGAS entrained-flow gasifier located in Puertollano, Ciudad Real (Spain). This material was provided in the summer of 2009 and, due to the considerable amount of wastes produced by the plant and due to the variability of the operating conditions of the gasifier, it might not be fully representative of the ash generated by the industrial gasifier during normal operation.

A preliminary elemental analysis on slag and slag fines revealed no appreciable carbon content (for the former) and a carbon content as high as 57.4% (for the latter). While elemental analysis on slag did not highlight the presence of carbon in this material, interestingly, different results were obtained when cross-sections of coarse slag particles were analyzed by Scanning Electron Microscopy/Energy Dispersive X-ray (SEM-EDX) analysis (Fig. 1a; EDX results not listed for the sake of brevity). The whole slag particle shown in Fig. 1a appeared to be mostly vitreous and dense. While the inorganic fraction is primarily constituted by Si+Al (47.5%), a considerable amount of carbon (9.3%) could also be detected. Figs. 1b–c report SEM results obtained carrying out the analysis at a greater magnification on the cross-section of two selected zones of slag particles. In both cases the occurrence of darker *patches* (see Fig. 1b and 1c) was observed. Quantitative EDX results refer to these regions: C-contents as high as 48.8–54.2% were obtained. This finding contributes to the assessment of the relevance of carbon entrapment in slag particles. It is worth noting that elemental analysis did not show the presence of any organic fraction and this was essentially because C was permanently embedded into the slag matrix in a way that could not have been disclosed by thermal analysis. Only the cutting procedure associated with the SEM-EDX analysis was able to disclose the unreacted carbon, which appeared to be somewhat segregated (in the *patches*) with respect to the inorganic slag matrix. Fig. 2 reports the results of the SEM analysis performed on whole slag fines particles. In particular, particles having prevailing either porous (Figs. 2a–c) or compact (Figs. 2d–e) structures were observed. In any case, the carbon content was larger than the value obtained from the inspection of coarse slag particles, in line with results of elemental analysis. This is particularly evident for porous particles (Figs. 2a–c): C-content ranged between 82.3 and 86.5%. Thus, these particles should be mainly associated with unreacted char present in the dense-dispersed phase giving rise to slag fines upon impingement on the quench bath. On the other hand, dense particles (Figs. 2d–e) display morphological and chemical features that are closer to coarse slag particles, at least as far as SEM-EDX results are concerned: C-content ranged between 13.9 and 18.4%, and the Si+Al-fraction was as high as 33.1–35.0%. These results are consistent with the previously-reported C-content of slag fines (about 57%), obtained by standard elemental analysis carried out on waste containing both high-C porous and low-C dense materials. Moreover, the more compact slag fines should be regarded as having intermediate properties between porous slag fines and coarse slag: this observation highlights again the establishment of a dense-dispersed phase that, together with the slag phase, generates both streams: slag and slag fines, the latter being characterized by a mean particle size and density around 100 μm and 1000 kg m^{-3}, respectively.

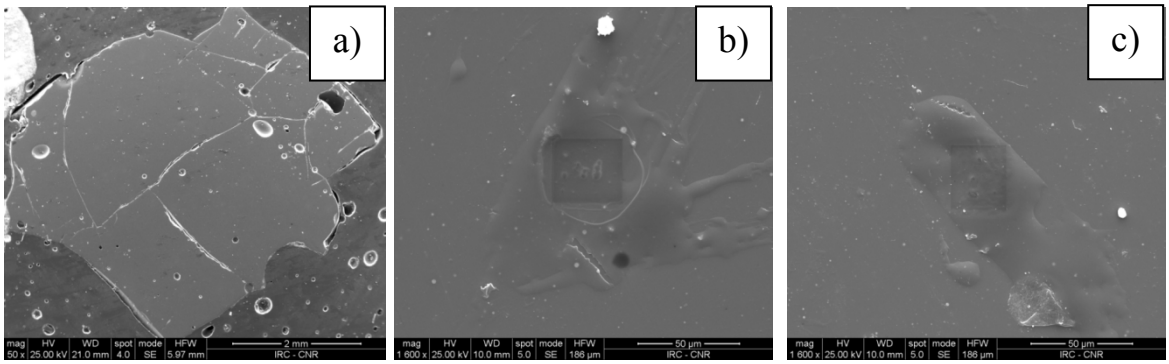

Figure 1. SEM micrographs of cross-sections of: a) a whole coarse slag particle (magnification = 50×); b)–c) selected zones of slag particles (magnification = 1600×) displaying carbon-rich patches.

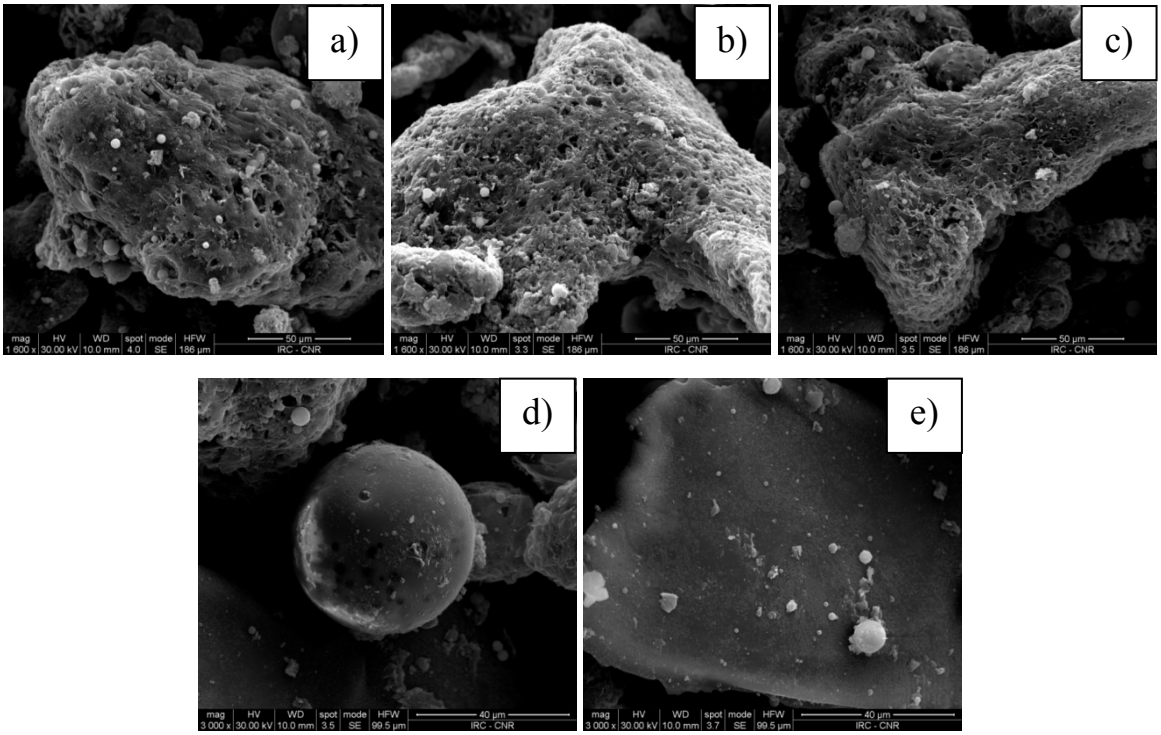

Figure 2. SEM micrographs of different whole slag fines particles: a)–c) at magnification = 1600×; d)–e) at magnification = 3000×.

Numerical Model

The migration of char particles on the wall slag layer is influenced by the turbulence and centrifugal forces induced by swirled or tangential motion imposed to the inflowing gas. A time-dependent description of the turbulent boundary layer that drives the interaction of the flying particles with the slag is preferred with respect to a time-averaged approach in order to model the mechanisms of char particles deposition. Numerical modelling of the gas-solid multiphase flow is performed adopting an Eulerian-Lagrangian approach. The Eulerian fluid phase is modelled by the space-filtered Navier-Stokes equations, following the LES approach to take into account the effects of turbulence. OpenFOAM [19] is the numerical code adopted to obtain the numerical solution of the modelling equations. Details on the mathematical model and numerical approach can be found in a separate paper [14]. Here it is only recalled that the equations for a weakly-compressible fluid flow are solved adopting a semi-implicit,

pressure-velocity, iterative solution method (PISO), with the aim of setting up a model that could easily be applied to realistic conditions of non-uniform temperature and variable gas density. Gravity force is not considered in the momentum equation. The gas is modelled under perfect gas assumption. In summary, model equations for the gas phase are the Favre-filtered balance equations for mass, momentum and energy. Closure of Sub Grid Scale (SGS) terms is provided adopting the compressible version of localized dynamic model LDKM developed by Kim et al. [20]. According to such formulation, an additional transport equation is considered to compute the evolution of the subgrid turbulent kinetic energy k^{sgs}. Constants appearing in this model are evaluated according to a dynamic-based procedure [21]. Thus, the model is supposed to tune the effects of the subgrid scales on the resolved field during the computation. Such feature overcomes the limitations based on the assumption of local equilibrium of energy transfer between the scales separated by the filter cut-off at which Smagorinsky eddy viscosity closure is defined. Periodic boundary conditions for k^{sgs} are assigned along the turbulence homogeneous directions, while zero value for k^{sgs} is assigned on the solid walls.

The Discrete Element Method is adopted for the solid phase, solving the equation of motion for each single particle included in the domain, following a Lagrangian Particle Tracking (LPT) method. Tracked particles are considered point-wise. They are assumed to be rigid hard spheres subjected only to a Stokes drag force. The relation between the drag coefficient and the particle Reynolds number is assigned according to classical correlations. A simple one-way coupling with the fluid motion is supposed. It is known that such a model is not able to accurately capture the motion of lighter particles near the walls [22]. Therefore, present results are not able to give accurate quantitative predictions of the deposition rate and accumulation of particles near the wall. However, as the main goal of the study was that of highlighting the behaviour of particles upon impact with the wall at particle velocities of the order of the bulk flow velocity, i.e. under conditions of relatively high particle inertia, the present model is considered sufficiently accurate, particularly for the heavier particles. Accordingly, the real structure of the dense and thin film of solid particles accumulating near the wall and not entrapped into the slag cannot be reproduced, limiting the present analysis to the incipient formation of such a layer. Second-order accurate schemes have been selected with reference to both time and space, ensuring the required accuracy for an LES. Comparison of the results with a well-established benchmark will be presented thereafter to establish the level of accuracy obtained.

Parametric Analysis from Numerical Results: Effect of Stokes Number and Restitution Coefficient in Planar and Curved Geometries

The effects of two main parameters will be considered in this study: the wall impact restitution coefficient and the particle's inertia. The first is relevant to the different role that the presence of the slag or the film of segregated particles already deposited can play upon the rebound of the impinging particles. The second is essential to reproduce the conditions at which particles impinge onto the confining gasifier's walls, dragged by the swirled or tangential flow. Results will be separately discussed for the two different flow geometries considered, i.e. planar and curved channel.

Planar Channel Flow

The effect of the restitution coefficient (ε, which is equal to 1 for complete restitution of particles momentum, i.e. elastic impact) and of the particle Stokes number on the establishment of different flow structures close to the slag layer has been investigated by performing simulations of the particle-laden flow in a planar channel geometry. A sketch of the geometry and dimensions is given in Fig. 3. The flow in the periodic channel is sustained

by a mass body force, resembling the form of a pressure gradient, introduced in both the momentum and energy equations to ensure the desired mass flow rate and consequently the wall shear stress, determined by a fixed value of the Reynolds number $\mathrm{Re}_\tau = h\,\rho\,u_\tau/\mu$, where ρ and μ are the gas density and viscosity, respectively, and u_τ is the friction velocity [23]. Having imposed a constant pressure gradient to sustain the flow in the channel, in the incompressible limit the mean friction velocity is consequently fixed. Simulations have been performed at $\mathrm{Re}_\tau = 150$. Flow properties are fixed to those of air at ambient conditions. The corresponding Mach number is M = 0.005. Initial conditions for velocity are represented by a parabolic profile perturbed along the streamwise and spanwise direction in order to promote transition to turbulent regime. The initial temperature profile is assigned to impose a non-zero heat flux through the boundaries using the laminar distribution. Isothermal and no-slip boundary conditions are used on the solid walls. Turbophoresis effects of the fluid phase on particle motion are very sensitive to the dimension of the resolved scale: so, to correctly model the particle-wall interaction phenomena, there is the need of a very good resolution of the mesh size near the wall. A grid refinement sensitivity analysis has been performed with two grids, having 32×32 equal cells in the x and z direction and 64 cells in the y direction, with length geometrically graded from the walls to the center of the channel. Subsequently, the number of cells in the domain was increased to a matrix of 48×48×96 cells in the x, z and y direction, respectively. Up to the previously selected grid resolution, the advective stability constraint on time discretization step was ensured by selecting $\Delta t = 2\times10^{-4}$ s on the finer grid. This simulation corresponds to the setup chosen for a well-established benchmark [24] and it allows to assess the accuracy of the method here proposed. Simulations have been run for a very long time of 1800 s.

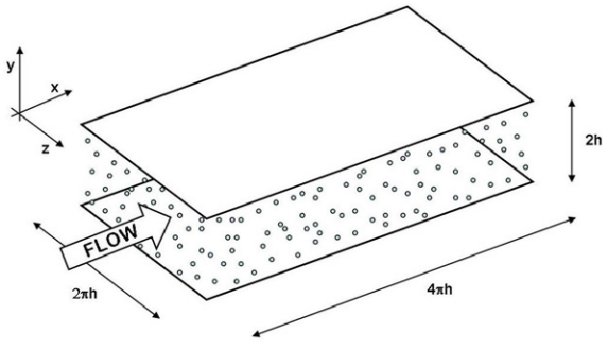

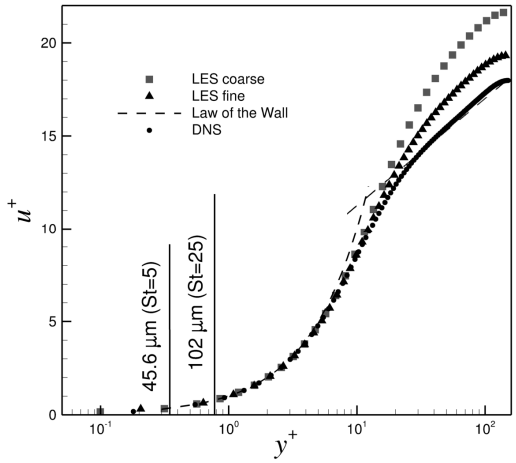

Figure 3 (left). Sketch of the planar channel flow geometry with indication of the dimensions adopted (h = 0.02 m).

Figure 4 (right). Mean velocity profiles in the periodic planar channel flow geometry; the diameter of the particles laying onto the wall is also reported, together with their Stokes number.

Fig. 4 shows the semilog plot of non-dimensional averaged streamwise velocity profiles, $u^+ = u/u_\tau$, versus the wall-normal non-dimensional coordinate in wall units, $y^+ = y\,\rho\,u_\tau/\mu$, for two different grid refinements (LES coarse and LES fine). It is here recalled that $y^+ = 0$ and $y^+ = \mathrm{Re}_\tau = 150$ correspond to wall and mid-channel positions, respectively. For the finer grid, results compare well with the reference profiles obtained by Direct Numerical Simulation (DNS) [24]. For this grid, the Δy^+ of the first cell center near the wall is about 0.2, and at the

center of the channel it is about 21. Once fully-developed flow conditions are reached, two different clouds of 10^5 particles having density 10^3-times that of the gas and diameter chosen such that the particle Stokes number for each cloud were equal to 5 and 25, respectively, are placed in the overall channel, randomly spaced along the x, y and z direction, and they are all tracked independently. The initial particles velocity equals the fluid velocity at the same positions, and their density (around 1000 kg m^{-3}) and diameter (around 50-100 μm) are consistent with properties of slag fines, as previously discussed.

In Fig. 5 the average particle concentration α along the channel height y^+ at the end of the simulation is reported, for different grid resolutions (LES coarse and LES fine), values of the restitution coefficient (0.2 and 1) and Stokes numbers (5 and 25). The concentration α is normalized with respect to the initial concentration α_0. First of all, in Fig. 5 (left) it is observed that the concentration is quite sensitive to the distribution of the slices thickness adopted, by holding the ε-value. The same distribution considered by Marchioli et al. [24] has been here adopted to allow direct comparison with benchmark results. Only the results obtained with the finer mesh are in satisfactory agreement with reference DNS literature data [13,25]. Thus, for further results only the finer grid has been considered. As a general comment, in any case the particle concentration is maximum near the wall to rapidly decrease toward the channel centre. For each value of the Stokes number, limited effect of the restitution coefficient is observed, when switching from a complete ($\varepsilon = 1$) to partial ($\varepsilon = 0.2$) restitution. The particle concentration near the wall is as high as nearly 4- and 180-times the initial value α_0 for the case of St = 5 (finer particles, Fig. 5 (left)) and St = 25 (coarser particles, Fig. 5 (right)), respectively.

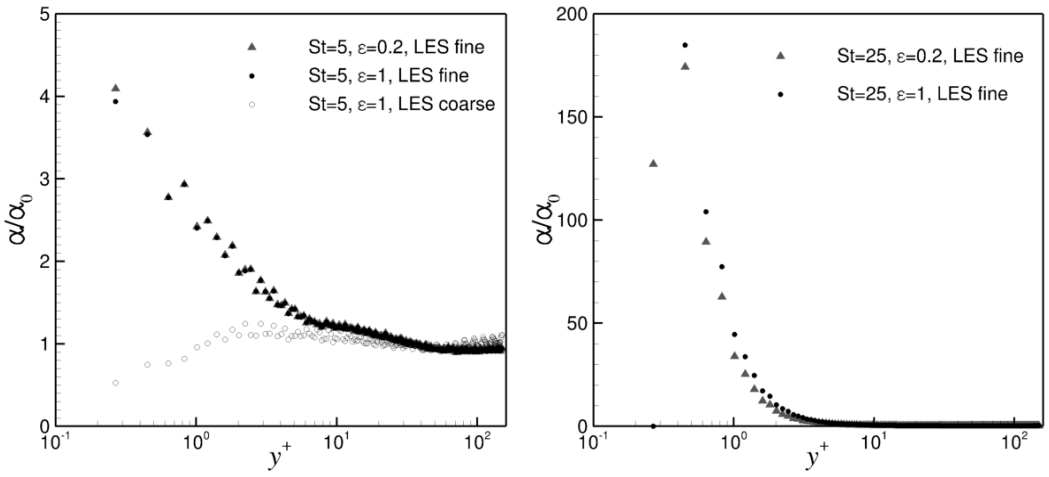

Figure 5. Average particle concentration along the planar channel height at St = 5 (left) and St = 25 (right), for different grid resolutions and values of the restitution coefficient ε.

The variation of the maximum particle concentration (that is, the value establishing near the wall) versus time is reported in Fig. 6 (left). For both values of St, two distinct regions can be recognized. The first extends from the injection time up to few tens of seconds. During this time particle transfer toward the walls approaches completion. After a few tens of seconds the time-series are characterized by oscillations of the maximum concentration around values of α/α_0 equal to about 4 and 180 for St = 5 and St = 25, respectively. Again, no marked effect of ε was recognized, while the greater extent of near-to-wall segregation of coarse particles upon impingement on the slag layer is confirmed.

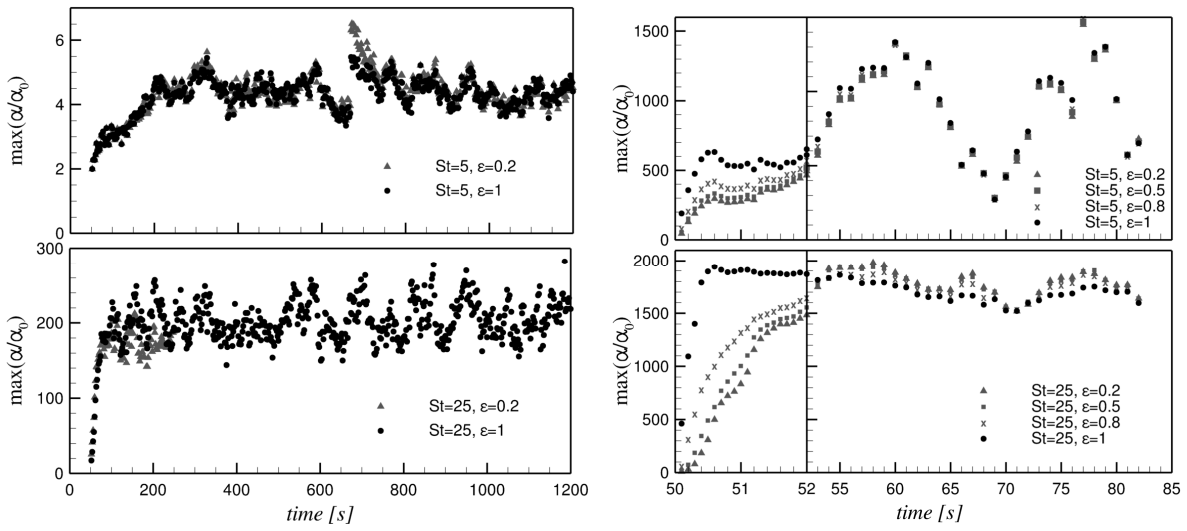

Figure 6. Maximum average particle concentration versus time at St = 5 (top) and St = 25 (bottom) for different values of the restitution coefficient ε. Left: planar channel domain. Right: curved channel domain.

Curved Channel Flow

In order to evaluate the particle-wall dynamics under the action of a non-parallel flow, which could better reproduce the tangential flow establishing in a gasification chamber, a different configuration was also studied. The new configuration (Fig. 7 (left)) is formed by a curved periodic channel. This is a portion of volume between two co-annular cylinders, the outer having a radius R = 0.096 m, equal to the radius of the Sommerfeld and Qiu [26] experimental setup. The inner cylinder has a radius such that the distance between the two cylinders is 2h. The external cylinder acts as a fixed confining wall while the inner rotates to set the fluid in motion. Periodic conditions are applied to both the radial confining planes and to the z normal bounding planes. The grid size closely resembles that adopted for the planar channel flow configuration, having considered the same number and spacing of grid points. This configuration corresponds to a portion of the rotating Couette flow [27], that develops instability waves appearing in the form of flow vortices reported in the cross-sectional map of the flow field shown in Fig. 7 (right), where a contour plot of u_y, i.e. the component of the instantaneous velocity normal to the wall, is reported. This component is significant when compared with the magnitude of the velocity u_{mag}, also reported in Fig. 7 (right) in a cross-section orthogonal to the z-axis. This component exerts a pronounced drag on particles which extensively transports them from one wall to the other. In this way, the total drag force accelerates the particles with components tangential to the wall and normal to the wall. The inertia that particles gain can be controlled, to some extent, by changing the rotation velocity of the inner wall, here fixed to 72 rad s^{-1}. The fully-developed flow shows a value of the wall normal shear stress corresponding to a value of Re_τ = 120, comparable to that of the planar channel.

In Fig. 6 (right), it is possible to observe the effect that a larger inertia of particles has on the different rates of particle deposition. The figure reports the maximum value of the particle concentration observed near the outer wall as a function of time. Similarly to the case of the planar channel flow (Fig. 6 (left)), the flow is fully developed before particles are injected with a velocity equal to that of the flow at the same position at t = 50 s, at randomized locations. Almost all the particles accumulate on the outer side of the domain, due to the effect of centrifugal forces. Starting from t = 50 s, two distinct time intervals can be identified for both values of St. During the first interval, spanning about two seconds and highlighted in

the figure by expanding the time scale, particles rapidly move towards the outer wall. This is qualitatively analogous to what observed in the planar channel case, but it is remarkable that the values of the maximum concentration are now much larger, for the same values of St and ε. Moreover, a new feature is recognized, i.e. that the restitution coefficient now shows a marked effect (the higher the coefficient, the higher the maximum concentration). After this first time interval, however, the particles approach a behaviour which qualitatively resembles that of the planar case. The maximum concentration of particles oscillates around an α/α_0-value that is about 1000 and 1800 for St = 5 and St = 25, respectively, nearly independent from ε in the range investigated. Coarser particles show larger maximum concentrations, but the sensitivity of the maximum particle concentration upon particle diameter is smaller than in the planar case. Oscillations of the maximum concentration of solids near the wall indicate that the structure of particle clusters induced by accumulation is not steady, and is largely influenced by large-scale flow structures.

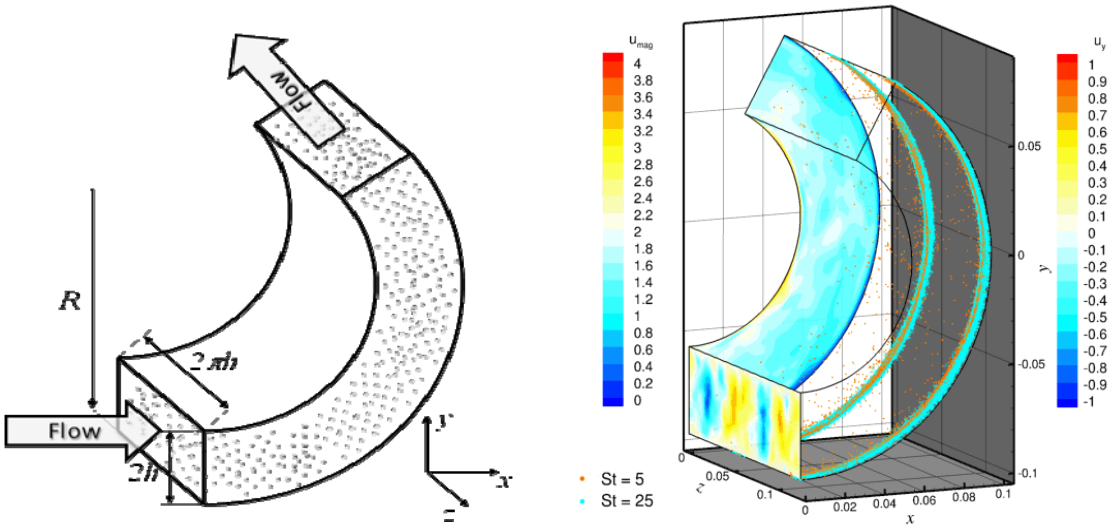

Figure 7. Left: sketch of the curved channel flow geometry with indication of the dimensions adopted (h = 0.02 m). Right: computed distribution of particles after 80 s from injection, for either St = 5 or St = 25 and ε = 1, together with the instantaneous velocity field (values in m s^{-1}).

Discussion

Numerical results show that, invariably with the chosen parameters, particle concentration near the wall in all the simulated cases does not appear perfectly steady. The spatial distribution of the particles near the wall, as appearing from snapshots in the case of the planar channel flow, is reported in Fig. 8. Different levels of clustering are clearly recognizable, for instance looking at the regions indicated with letters A and B. The maximum local particle concentration shows values significantly higher than the previously reported averaged values, with local clustering emphasized in the case of lower values of ε. A similar but even more enhanced behaviour is observed in the curved channel flow, as clearly recognizable in Fig. 7 (right). Results for this case suggest that, even when surface particle distribution is fully governed by turbophoretic effects, different levels of segregation can coexist, shedding doubts on models that assume uniform particle deposition rates onto the slag. Furthermore, the presence of dense particle clusters introduces a kind of "roughness" into the limiting gas/slag interface, that can be expected to impact the particle segregation mechanism. This behaviour cannot be simulated with the current version of the model, as it

would be necessary to take into account both particle-particle interaction and the effects of particles on the fluids in both the density and momentum balances.

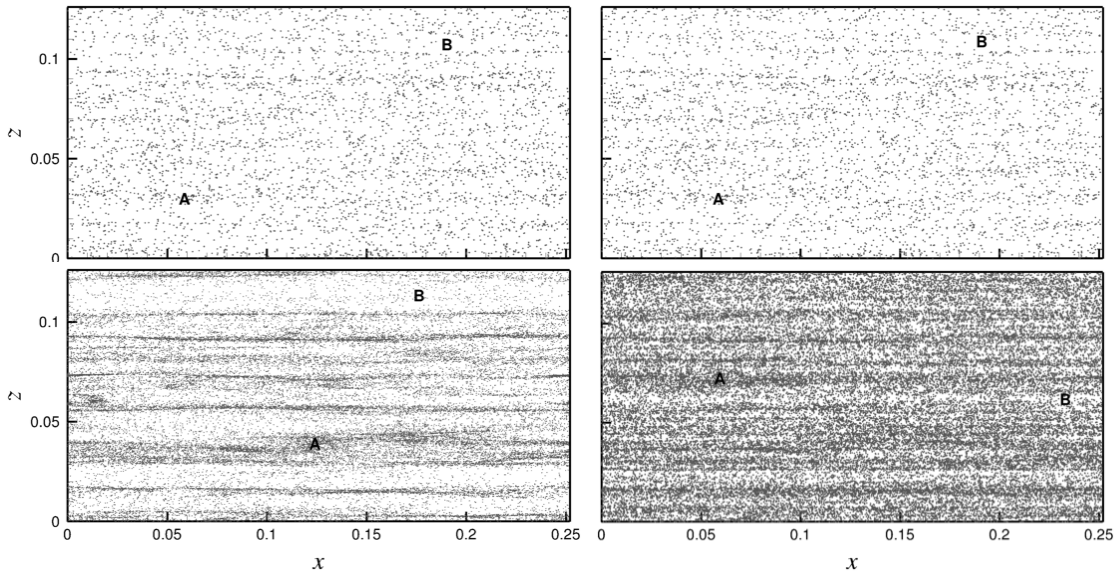

Figure 8. Snapshots of the particles distribution near the wall (maximum distance less than 1 mm) after 1200 s from injection. Planar channel flow case. Top (left and right): St = 5. Bottom (left and right): St = 25. Left (top and bottom): $\varepsilon = 0.2$. Right (top and bottom): $\varepsilon = 1$.

On the other hand, numerical simulation results do confirm the establishment of a region near the wall slag layer (the dense-dispersed annular phase referred to in the Introduction, leading to the formation of the slag fines), in which particles impacting the slag accumulate to an extent depending on the system fluid-dynamics and on parameters such as particles Stokes number and restitution coefficient. Interestingly, the segregation of char particles near the wall is more evident for the curved channel flow geometry, a more realistic case, and is enhanced for coarser particles. Particle accumulation appears to take place within a relatively short time since particle injection. The establishment of this dense-dispersed phase is considered to be beneficial to carbon gasification, due to the increased mean residence time in the gasifier of char particles belonging to this phase.

Conclusions

Analysis of slag samples taken from the quench/drain bath of a full-scale entrained-flow slagging gasification plant suggests the existence of two phases: coarse slag granules and slag fines. Carbon occurs very occasionally in coarse slag samples, as embedded patches incorporated into the resolidified molten ash. Slag fines are porous and very rich in carbon. The existence of the two phases is consistent with a phenomenological framework according to which a dense-dispersed particle-laden flow establishes close to the gasifier wall as a consequence of particle accumulation promoted by turbophoresis and inertial forces.

The mechanism of near-wall accumulation of particles from particle-laden streams has been studied by detailed numerical simulations of the two-phase flow in the proximity of the slag-covered gasifier's walls. The influence of the planar versus curved geometry of the flow field, of the particle Stokes number, of the coefficient of restitution upon particle impacts against the boundary has been investigated. Numerical results confirm that near-wall accumulation of particles may be extensive, promoted by the curved geometry, by large

Stokes number typical of coarse particles, by small coefficient of restitution. The relevance of near-wall particle segregation on the performance of entrained-flow gasifiers is confirmed.

Literature Cited

[1] Wilcox, D.C., *Turbulence Modelling for CFD*, DCW Industries Incorporated, 2006.
[2] Sagaut, P., *Large Eddy Simulation for Incompressible Flows*, Springer, 2001.
[3] Walsh, P.M., Sarofim, A.F., Beér, J.M., *Energy Fuel.* 6: 709–715 (1992).
[4] Shimizu, T., Tominaga, H., *Fuel* 85: 170–178 (2006).
[5] Montagnaro, F., Salatino, P., *Combust. Flame* 157: 874–883 (2010).
[6] Bockelie, M., Swensen, D., Denison, M., Chen, Z., Maguire, M., Sarofim, A., Yang, C., Shim, H.S.A., *Computational Workbench Environment for Virtual Power Plant Simulation*. *Quarterly Progress Report*, Reaction Engineering International, 2004.
[7] Wang, H., Harb, J.N., *Prog. Energy Combust. Sci.* 23: 267–282 (1997).
[8] Seggiani, M., *Fuel* 77: 1611–1621 (1998).
[9] Lee, F.C.C., Lockwood, F.C., *Prog. Energy Combust. Sci.* 25: 117–132 (1999).
[10] Wang, X.H., Zhao, D.Q., He, L.B., Jiang, L.Q., He, Q., Chen, Y., *Combust. Flame* 149: 249–260 (2007).
[11] Uijttewaal, W.S.J., Oliemans, R.V.A., *Phys. Fluids* 8: 2590–2604 (1996).
[12] Kuerten, J.G.M., *Phys. Fluids* 18: 025108 (2006).
[13] Marchioli, C., Salvetti, M.V., Soldati, A., *Acta Mech.* 201: 277–296 (2008).
[14] Ambrosino, F., Aprovitola, A., Brachi, P., Marra, F.S., Montagnaro, F., Salatino, P., *Proc. 12th Int. Conf. Multiphase Flow in Industrial Plants*, Ischia, Italy, paper submitted (2011).
[15] Montagnaro, F., Brachi, P., Salatino, P., *Submitted for publication* (2011).
[16] Wu, T., Gong, M., Lester, E., Wang, F., Zhou, Z., Yu, Z., *Fuel* 86: 972–982 (2007).
[17] Xu, S., Zhou, Z., Gao, X., Yu, G., Gong, X., *Fuel Process. Technol.* 90: 1062–1070 (2009).
[18] Zhao, X., Zeng, C., Mao, Y., Li, W., Peng, Y., Wang, T., Eiteneer, B., Zamansky, V., Fletcher, T., *Energy Fuel*. 24: 91–94 (2010).
[19] OpenCFD, *OpenFOAM Programmers Guide* (2008).
[20] Kim, W.W., Menon, S., Mongia, H.C., *Combust. Sci. Technol.* 143: 25–62 (1999).
[21] Germano, M., Piomelli, U., Moin, P., Cabot, W.H., *Phys. Fluids* A3: 1760–1765 (1991).
[22] Kuerten, J.G.M., Vreman, A.W., *Phys. Fluids* 17: 011701 (2005).
[23] Lenormand, E., Sagaut, P., Ta Phuoc, L., *Int. J. Numer. Meth. Fl.* 32: 369–406 (2000).
[24] Marchioli, C., Soldati, A., Kuerten, J.G.M., Arcen, B., Tanière, A., Goldensoph, G., Squires, K.D., Cargnelutti, M.F., Portela, L.M., *Int. J. Multiphas. Flow* 34: 879–893 (2008).
[25] Marchioli, C., Salvetti, M.V., Soldati, A., *Phys. Fluids* 20: 040603 (2008).
[26] Sommerfeld, M., Qiu, H.H., *Int. J. Multiphas. Flow* 19: 1093–1127 (1993).
[27] Tritton, D.J., *Physical Fluid Dynamics*, Clarendon Press, 1988.